

Flat Specimen Shape Recognition Based on Full-Field Optical Measurements and Registration Using Mapping Error Minimization Method

Andraž Maček – Janez Urevc – Miroslav Halilović*

University of Ljubljana, Faculty of Mechanical Engineering, Slovenia

In the paper, an alignment methodology of finite element and full-field measurement data of planar specimens is presented. The alignment procedure represents an essential part of modern material response characterisation using heterogeneous strain-field specimens. The methodology addresses both the specimen recognition from a measurement's image and the alignment procedure and is designed to be applied on a single measurement system. This is essential for its practical application because both processes, shape recognition and alignment, must be performed only after the specimen is fully prepared for the digital image correlation (DIC) measurements (white background and black speckles) and placed into a testing machine. The specimen can be observed with a single camera or with a multi-camera system. The robustness of the alignment method is presented on a treatment of a specimen with a metamaterial-like structure and compared with the well-known iterative closest point (ICP) algorithm. The performance of the methodology is also demonstrated on a real DIC application.

Keywords: full-field measurements, digital image correlation (DIC), specimen shape recognition, surface registration, iterative closest point (ICP)

Highlights

- A methodology is proposed for aligning FEA data and the full-field measurement data of planar specimens.
- The methodology offers both the shape recognition and alignment process to be performed on a single full-field measurement system.
- The main advantage of the proposed methodology is its robustness.
- The performance of the methodology is presented on synthetic as well as real DIC data.
- The measured specimen can be observed with a single camera or a multi-camera system.

0 INTRODUCTION

Advanced constitutive models allow precise adjustment of the material mechanical response to specific loading conditions. Their flexibility is a result of a large number of free parameters. However, as the number of parameters increases, information gathered from standard experiments becomes insufficient or a huge amount of different experiments is required [1] and [2]. An alternative to the approach is taking into account the full-field kinematic information. Such data are normally acquired through digital images from where the displacement fields can be calculated using the digital image correlation (DIC) techniques. The approach gives rise to the development of complex specimen shapes [3], making it possible to identify material parameters through a single experiment [4]. One of the challenges, still not sufficiently resolved and addressed in this work, is the alignment of planar specimens between the modelling (numerical) data and experimental DIC data.

Full-field measurements offer a huge amount of information on the specimen surface (several 10'000), especially compared to classical extensometers.

However, their dependency on the sought material parameters generally cannot be explicitly determined, and therefore direct material identification cannot be executed. Researchers resort to the use of inverse identification techniques, where the finite element model updating (FEMU) [5] represents one of the established methods with extensive research work performed on the full-field measurements [3] (e.g. DIC [6] response calculation or by employing different optimization methods (e.g. genetic algorithm [7] or simulated annealing [8])). The method is based on an iterative comparison between the measured and calculated specimen's responses. The optimal values of material parameters are then determined by minimizing their discrepancy.

However, before finite element model (FEM) results and DIC data can be compared, coordinate systems of both sets of data need to be aligned. The latest research shows that such alignment is essential for reliable identification of material parameters in the case of specimens with non-homogeneous strain field where sharp strain gradients occur. Fehervary et al. [9] examined material parameter fitting results of planar tests when the sample orientation was unknown

or deviated. The study showed that after a certain threshold of misalignment, reliable parameters can no longer be found. The authors also concluded that the level of threshold seemed to be material dependent. Lava et al. [10] studied two different methods used to compute full-field error maps between experimental DIC data and FEA data to, among others, investigate the effects of processing parameters, model form error (such as incorrect boundary conditions) and mesh alignment. The authors showed that even a small misalignment can have a surprisingly large effect on the strain error maps and exposed the necessity to develop robust and precise methods of alignment. Similarly, Ruybalid et al. [4] performed various virtual test cases to assess the performance of FEMU and integrated digital image correlation (IDIC) method when subjected to different error sources, among others, misalignment of the specimen. Both methods are shown to be sensitive to misalignment. Namely, the increase of the misalignment further increases the error on the identified material parameters.

It seems interesting that despite the importance of properly addressing the alignment of DIC and FEM data and considering the numerous publications addressing material characterization using planar specimens, not much information can be found on how researchers align both data sets in their works. However, as pointed out in a recent article from Polyga (a developer of 3D scanners with more than 10 years of experience), scanning flat objects can be particularly difficult even for experienced 3D scanning technician [11]. The process of aligning DIC in FEM data set generally consists of two steps, specimen's edge detection and alignment (point set registration). It is important to note that the procedure needs to be performed on the same optical system as DIC measurements so that the DIC and FEM data can then be compared, which adds to the complexity of the problem.

One of the best-known methods for point sets registration is the iterative closest point (ICP) algorithm introduced by Besl and McKey [12]. The algorithm consists of the closest point search and a minimization of the matching error, applied iteratively to the two surfaces to be matched [13]. Many variants of the algorithm have been introduced since, affecting the algorithm at different stages [14] and [15], e.g. the selection of points, matching, rate of convergence, etc. However, despite the widespread of the ICP method, its convergence in the general case of initial misalignment cannot be guaranteed [16]. Also, optical full-field displacement measuring methods most

commonly cannot accurately measure the specimen shape.

To address the problem of aligning full-field measurements with FEM data, Bruno et al. [17] utilized a linear transformation matrix to map the location of the calculation point into the measurement picture pixel position. The projection matrix was determined using user input coordinates of the calculation point and the pixel positions of three arbitrary points. The spatial position of all three points must be known a priori and all of them must be observed by the measurement. A similar approach was employed by Silva [18] who transformed the model coordinate system by recognizing that some reference points observed in the image have known numerical coordinates. Both calibration procedures are easy to implement but with the state of the art specimen designs, which exhibit smooth shapes and no dominant features [19] they become increasingly difficult to be used and prone to errors.

In the present work, a robust methodology is presented for aligning full-field measurements (e.g. DIC) and modelling (e.g. FEM) data of flat specimens. The procedure addresses both the contour recognition of a specimen as well as registration. Namely, for a successful DIC measurement, the specimen must be covered with a speckle pattern consisting of a white background and black speckles. In practice, this represents a problem because the distinction between the specimen and the background can quickly be lost. We determine the specimen's geometry by taking two consecutive images with changing the background illumination. From their comparison, the background can be subtracted, leaving just the specimen's geometry. The result is a black-white image of the measured specimen (white) and the background (black). To perform the alignment, the CAD model is also projected onto the image as black and white pixels. By minimizing the intersection between both images, i.e. the measured specimen and numerical model, both data sets are aligned.

In the following, the methodology is presented first in the case of 2D and then 3D measurements. The performance of the method is demonstrated on two examples. In the first example, a synthetic one, we demonstrated the method on a problem of aligning a specimen with a metamaterial-like structure. In the example, we also analyse the effect of misalignment and compare the performance of the method with the ICP. In the second example, the method is demonstrated on real DIC data where its ability to handle the presence of noise and mismatches in the geometry is also presented. Discussion of the

results and the performance of the method is given in the Discussion section, which is followed by the conclusion.

1 METHODS

The method will be presented first in the case of 2D DIC measurements, where the specimen is observed with a single camera, located normal to its front surface (Fig. 1a). Afterwards, the method will be generalized for the case of 3D DIC measurement. Although in the latter case, additional coordinate transformations are needed to take into account the specimen's perspective (Fig. 1b), the alignment procedure is in both cases the same.

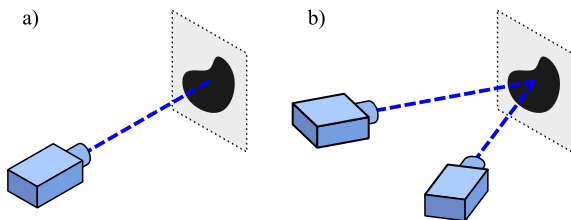


Fig. 1. Camera arrangement for a) 2D, and b) 3D DIC measurement

1.1 2D measuring System

Specimen recognition. Let us denote the numbering of pixels in the acquired (DIC) image in a form of a set:

$$P = \{(u, v) \in \mathbb{N} \times \mathbb{N} \mid u \leq n \text{ and } v \leq m\}, \quad (1)$$

with the size of the image being $n \times m$ pixels.

To determine the set of pixels which represent the specimen surface, two images of the same specimen are needed. The first image is a regular one used for the measurement itself. The background on the acquired image is usually dark and cannot be clearly distinguished from the specimen. For the second image, we brighten up the background using an illumination panel, as shown schematically in Fig. 2 by the two left-most images (corresponding to specimen recognition).

The region of the specimen, which we wish to determine, is defined by a set $S_m \subset P$, which is a set of pixels, whose difference in grayscale values between both images is below a threshold value ε :

$$S_m = \{(u, v) \in P \mid |g_1(u, v) - g_2(u, v)| < \varepsilon\}, \quad (2)$$

where $g_1(u, v)$ and $g_2(u, v)$ represent grayscale values of the $(u, v)^{\text{th}}$ pixel in the individual image, respectively.

Alignment. First, positions of pixels (u, v) of the specimen's shape (set S_m) need to be transformed into a physical location associated with specimen dimensions (X, Y) , see Fig. 2. This is performed with a calibration procedure, which can be written in a form of an arbitrary function c

$$c: \mathbb{N}^2 \rightarrow \mathbb{R}^2; (u, v) \mapsto (X, Y). \quad (3)$$

By assuming that the position of the camera is normal to the specimen surface and neglecting the optical distortions [20], the calibration only scales (u, v) as

$$\begin{Bmatrix} X \\ Y \end{Bmatrix} = c(u, v) = k \begin{Bmatrix} v \\ n-u \end{Bmatrix}, \quad (4)$$

with k being the scaling factor.

The relation between coordinates (X, Y) and the modelling space coordinates (x, y) can be written in a form of a mapping function f

$$f: \mathbb{R}^2 \rightarrow \mathbb{R}^2; (X, Y) \mapsto (x, y), \quad (5)$$

where the mapping, in general, carries out translational and rotational rigid body transformation only. For a planar case, we can write the mapping as

$$\begin{Bmatrix} x \\ y \end{Bmatrix} = f(X, Y) = \begin{bmatrix} \cos \alpha & -\sin \alpha \\ \sin \alpha & \cos \alpha \end{bmatrix} \begin{Bmatrix} X \\ Y \end{Bmatrix} + \begin{Bmatrix} \Delta x \\ \Delta y \end{Bmatrix}, \quad (6)$$

with α , Δx and Δy being the angle of rotation, translation in x and y direction, respectively. All three parameters $(\alpha, \Delta x, \Delta y)$ are unknowns and must be determined in such a manner that the modelling specimen, being in (x, y) space, coincides with the measured one, being in (X, Y) space.

So far, from the calibration and mapping procedure, one can determine each pixel location in the modelling space as $(x, y) = (f \circ c)(u, v)$. If we denote the specimen region in the (x, y) space as Ω_s (see Fig. 2), the set of pixels that are located inside the region Ω_s , denoted as a set $S_s \subset P$, follows as

$$S_s = \{(u, v) \in P \mid (f \circ c)(u, v) \in \Omega_s\}. \quad (7)$$

By comparing both images, the mismatch between the recognized measured and modelled specimen shape is determined as the symmetric difference between the two pixel sets S_m and S_s

$$E = S_m \Delta S_s. \quad (8)$$

Thus, E contains all the pixels of both sets S_m and S_s except for the ones in their intersection. The number of those pixels, i.e. the cardinality of the error set $|E|$, represents the measure of the mismatch level.

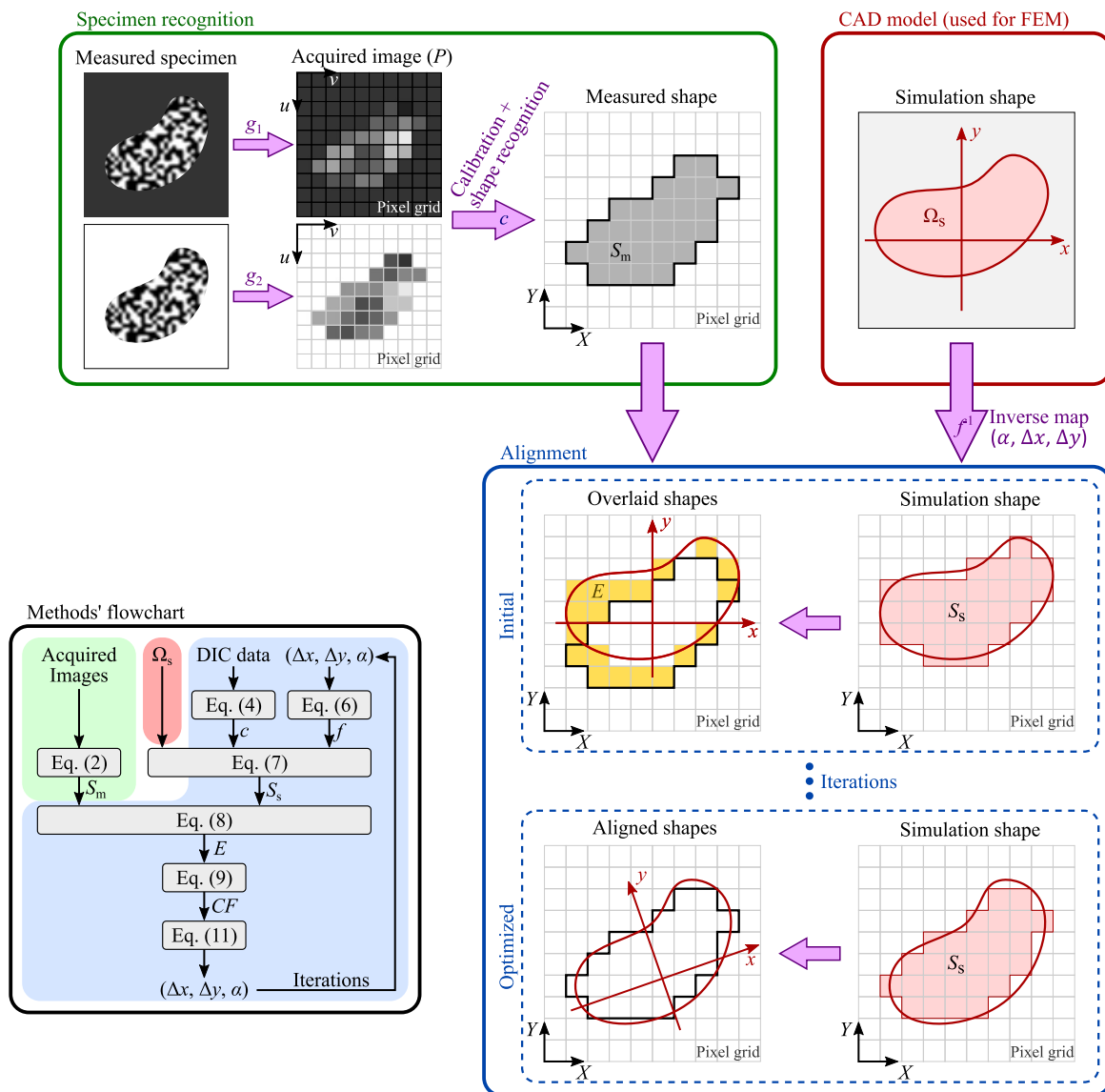


Fig. 2. The proposed alignment method

If the shapes are perfectly aligned, there will be no mismatched pixels, thus the cardinality of the error set would be zero.

The unknown mapping parameters $(\alpha, \Delta x, \Delta y)$ are determined as a solution to the following unconstrained optimization problem. Let us define the cost function $CF(\alpha, \Delta x, \Delta y)$ as

$$CF(\alpha, \Delta x, \Delta y) = |E|^2, \quad (9)$$

which needs to be minimized

$$\min CF(\alpha, \Delta x, \Delta y). \quad (10)$$

The result of the iterative optimization procedure (e.g. steepest descent method, Levenberg-Marquard algorithm) is a set of optimal values of mapping parameters $\{\hat{\alpha}, \hat{\Delta x}, \hat{\Delta y}\}$ that minimize the cardinality of the error set

$$\{\hat{\alpha}, \hat{\Delta x}, \hat{\Delta y}\} = \arg \min_{\{\alpha, \Delta x, \Delta y\}} CF(\alpha, \Delta x, \Delta y). \quad (11)$$

Once the optimal values of parameters are obtained, the measured results can be mapped into the modelling space via Eq. (6) as

$$\begin{Bmatrix} \hat{x} \\ \hat{y} \end{Bmatrix} = f(X, Y) = \begin{bmatrix} \cos \hat{\alpha} & -\sin \hat{\alpha} \\ \sin \hat{\alpha} & \cos \hat{\alpha} \end{bmatrix} \begin{Bmatrix} X \\ Y \end{Bmatrix} + \begin{Bmatrix} \hat{\Delta x} \\ \hat{\Delta y} \end{Bmatrix}. \quad (12)$$

1.2 3D Measuring System

The 3D measuring system consists of several digital cameras, each of them observes the specimen from its direction, as presented in Fig. 1b. The result of a 3D DIC measurement is a point cloud given in a measurement coordinate system $(\tilde{X}, \tilde{Y}, \tilde{Z})$, Fig. 3, which in general is not aligned with the specimen. In the case of planar specimens, a best-fit plane is normally constructed over the point cloud. The coefficients of the best-fit plane are determined using linear regression. Consequently, the location of the measured points in 3D $(\tilde{X}, \tilde{Y}, \tilde{Z})$ can be expressed with the 2D location on the best-fit plane (X, Y) . The reduction to 2D is essential to enable the use of equations derived in the previous subsection.

Calibration procedure c_i is performed for each camera with the purpose to map the pixels of the acquired images into the (X, Y) coordinate system. Each camera acquires its image with the corresponding pixel set P_i , $i = \{1, 2, \dots, N\}$ (analogously to Eq. (1)) with N being the number of cameras.

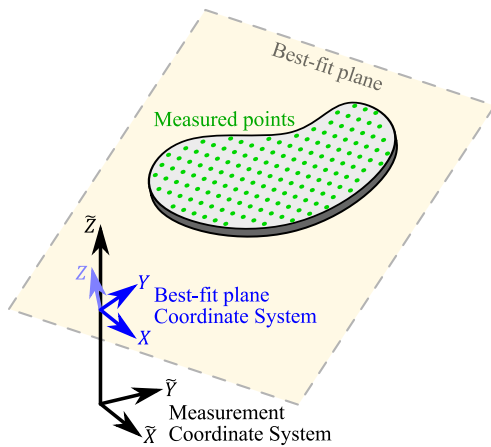


Fig. 3. Best-fit plane

The calibration procedure for each camera c_i is approximated using a linear transformation

$$\begin{cases} X \\ Y \end{cases} = c_i(u, v) = \begin{bmatrix} k_{uX,i} & k_{vX,i} \\ k_{uY,i} & k_{vY,i} \end{bmatrix} \begin{Bmatrix} u \\ v \end{Bmatrix} + \begin{Bmatrix} n_{X,i} \\ n_{Y,i} \end{Bmatrix}; \quad (13)$$

$(u, v) \in P_i$,

where k_* and n_* represent the constants of a two-dimensional linear function. Constants are obtained for each camera individually by employing two linear regressions. First regression calculates $k_{uX,i}$, $k_{vX,i}$ and $n_{X,i}$ by considering the known pixels' positions (u, v) and the corresponding position on the X axis of the best-fit plane. The second regression analogously

calculates $k_{uY,i}$, $k_{vY,i}$ and $n_{Y,i}$ by considering the known pixels' positions (u, v) and the corresponding position on the Y axis of the best-fit plane.

The mapping f of measured points on the best-fit plane (X, Y) to the modelling space (x, y) is performed as presented in the 2D case via Eq. (6). Sets $S_{m,i}$, $S_{s,i}$ and E_i , which again represent sets of pixels of the measured specimen, modelling specimen and the mismatch between the two, respectively, are constructed for each camera individually as already presented.

The level of the mismatch considering all cameras is expressed as the sum of all individual levels of mismatches squared

$$CF(\alpha, \Delta x, \Delta y) = \sum_{i=1}^N |E_i|^2, \quad (14)$$

with $CF(\alpha, \Delta x, \Delta y)$ being the cost function. As in the 2D case, optimal values of mapping variables $\{\hat{\alpha}, \hat{\Delta x}, \hat{\Delta y}\}$ are determined by minimizing CF . Measured data are then mapped onto the modelling space via Eq. (12).

2 EXPERIMENTAL INVESTIGATION

The performance of the method is presented on two examples. For a practical purpose, both examples are presented in the following along with the corresponding results. Discussion of results is then provided in Section 3. Minimization of the cost function (Eq. (10)) was in both cases performed using the steepest descent method. Derivatives of the cost function were approximated using the finite difference method.

In the first example, the synthetic one, we demonstrated the method on a problem of aligning a specimen with a metamaterial-like structure. The purpose of the experiment is to present the advantage of the proposed alignment algorithm in comparison with the well-known ICP algorithm. The effect of misalignment on the performance of methods is also studied.

In the second example, the entire methodology is presented on real DIC data (i.e. shape recognition and alignment), where the ability of the method to handle the presence of noise and mismatches in the geometry is also tested. The example presents a heterogeneous strain field specimen proposed for the calibration of plastic anisotropy.

2.1 Synthetic Experiment

The geometry of the specimen is shown in Fig. 4. The shape consists of cut-out slots exhibiting an even pattern, mimicking the shape of metamaterial [21].

The specimen in Fig. 4 also represents the reference (modelling) geometry. The measured geometry is obtained by introducing rigid translation and rotation to the reference one [10].

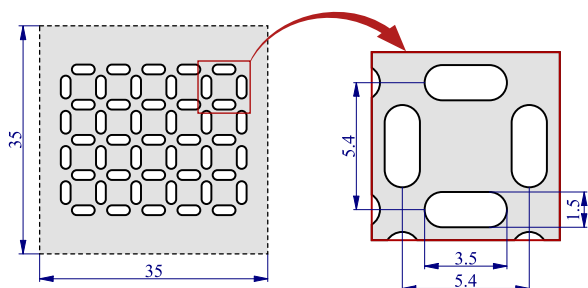


Fig. 4. Investigated synthetic specimen (dimensions in mm)

The effect of initial rotation and translation was examined to test the robustness of the method, mimicking multiple measurement setups. The translation was assumed equal in the horizontal x and vertical y direction (for the sake of brevity, to reduce the number of cases). Analysed cases include all possible combinations of rotations for angle α , ranging from 0° to 90° by a step 15° , and translations $\Delta x = \Delta y$, ranging from 0 mm to 2 mm with a step of 0.5 mm. An example of the initial misalignment ($\alpha = 2^\circ$, $\Delta x = \Delta y = 0.5$ mm), presents Fig. 5a. The corresponding error image, i.e. pixels from the error set E , Eq. (8), is presented in Fig. 5b in white.

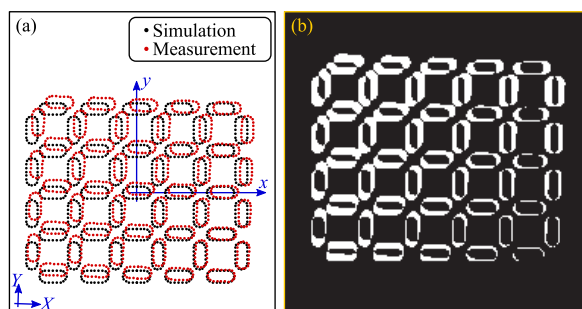


Fig. 5. Example of the analysed case:

- initial misalignment between simulation and measurement,
- the corresponding error image E , Eq. (8)

Besides the proposed method, the ICP was also employed in this example for comparison. Although many different versions of the ICP exist, one of the most basic closed-form versions of the algorithm was

assumed. Data used for the ICP are those presented in Fig. 5a. The closest point search was performed using the grid closest point and no false matches rejection was assumed.

Results. The performance of both methods is demonstrated by presenting the number of iterations that were needed to align each initial misalignment.

Results of both methods are presented in Fig. 6. Initial rotational misalignment α is displayed on the vertical axis and the translational Δx , Δy on the horizontal axis. Colours represent the number of iterations used for a successful alignment. Cases where the alignment was not achieved (exceeding 100 iterations or converged to an inappropriate position) are displayed in white.

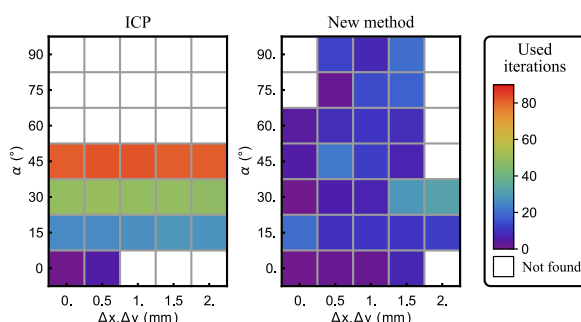


Fig. 6. Performance and convergence of ICP and the proposed alignment method

The proposed method managed to align the specimen in almost all the analysed cases of the initial misalignment. On the other hand, the ICP failed to converge or converged to a wrong minimum at initial misalignment rotations greater than 45° . With the increase of the initial rotation, the number of iterations considerably increased for the ICP, reaching over 80 iterations. The proposed method needed approx. 15 iterations on average for a successful alignment, irrespective of the initial rotation.

2.2 Application to Real DIC Data

Practical application of the method is demonstrated on a specimen presented in [22] (Fig. 7), designed to induce a biaxial strain-stress state. Due to the specimen's diverse geometry and no distinct features (such as sharp corners or round holes), the problem also represents a good alignment test problem.

Measurements were performed with a DIC measuring system Q-400 Dantec Dynamics GmbH, (Ulm, Germany). The measuring setup is presented in Fig. 8. We utilized 4 digital cameras, which in pairs acquire images of the front and

backside of the specimen, representing a case of a 3D DIC measurement. Such setup enables biplane measurement, where we simultaneously measure the front and back specimen surface in a common coordinate system. The calibration procedure was performed using a special two-sided calibration target. The purpose of such a set-up is enhanced characterization of material mechanical behaviour [22].

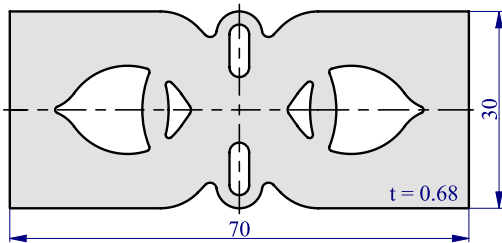


Fig. 7. Investigated specimen (dimensions in mm) [22]



Fig. 8. Measuring setup utilizing the digital image correlation

The DIC method was carried out with Istra 4D software. Technical details of the measuring system and the adopted DIC settings are summarized in Table 1.

The shape of the measured specimen was determined as presented in section Methods. Two images of the specimen were acquired by changing the background lightening as presented in Figs. 8 and 9. The first image was acquired using the typical lighting setup, presented on the left-hand side of Fig. 10a. For the second image, we illuminated the specimen from the backside, making the background on the acquired image brighter. The acquired image is presented on the right-hand side of Fig. 10a. The shape of the specimen is obtained from both images using Eq. (2).



Fig. 9. Image acquisition using a backlight

Table 1. Details of the measuring system

Company	DANTEC Dynamics GmbH, (Ulm, Germany)
Model	Q-400
Cameras	Manta G-507 (4 pieces)
Image resolution	2464 × 2056 pixel
Objective focal distance	35 mm
Field of view	approx. 65 mm × 40 mm
Patterning technique	mat white spray paint base coat with black speckles
Pattern feature size	approx. 3 pixel
DIC software	DANTEC Dynamics, Istra 4D (ver. 4.6)
Facet size	19 pixel
Grid spacing	12 pixel
Spatial smoothing	none
Temporal smoothing	none
Number of acquired data points	20400

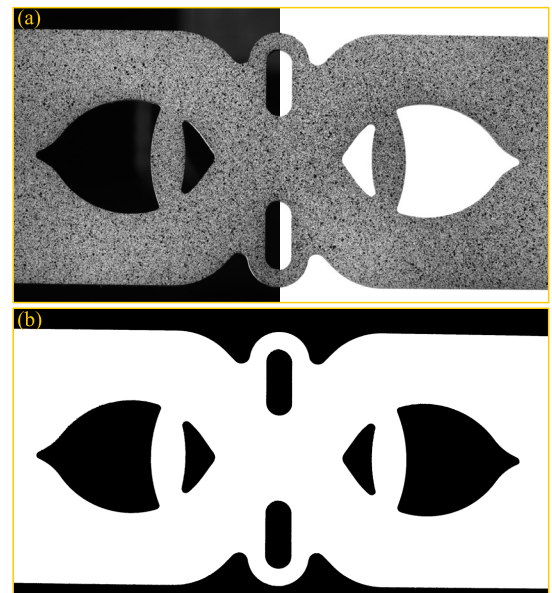


Fig. 10. Acquisition of specimen geometry: a) left-hand side: specimen image using typical lighting (Fig. 8) and right-hand side: using the backlight (Fig. 9), b) the obtained specimen geometry

Results. The determined shape of the measured specimen is presented in Fig. 10b. From the image, one could easily further determine the specimen contour, which most alignment methods use for the alignment procedure. In the proposed method, however, the entire shape is assumed, presented in Fig. 10b in white.

The measured and modelling specimen are together presented in Fig. 11a, given in the measured specimen's coordinate system. The measured shape is presented with the experimentally obtained image and the modelling shape with yellow dots. The corresponding error between both shapes is presented in the form of an error image, Fig. 11b. White pixels correspond to the error set E , obtained using Eq. (8), representing the regions of misalignment.

The initial value of the cost function CF , corresponding to the square number of white pixels in Fig. 11b, is approx. 10^{12} px^2 , Eq. (9). The value was then significantly reduced by the optimization procedure in only 5 iterations and the procedure successfully converged in 28 iterations. The final value of the cost function was reduced to approx.

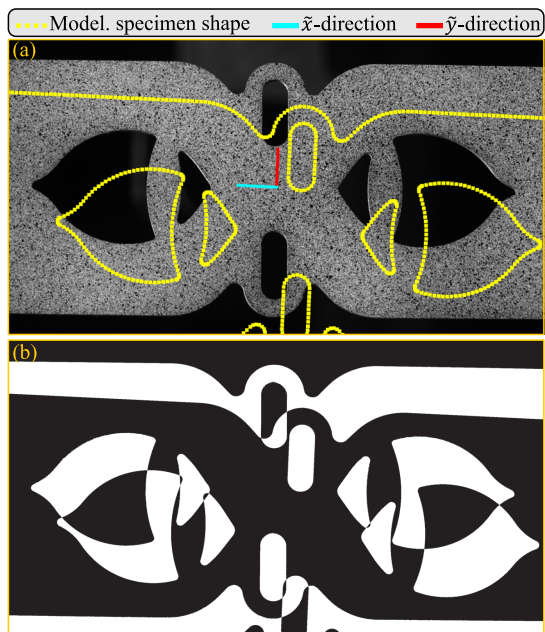


Fig. 11. The initial position of the measured and modelled specimen (the latter shown with yellow dots) in the measuring coord. system, a) presentation of both shapes, b) the corresponding error image of the method

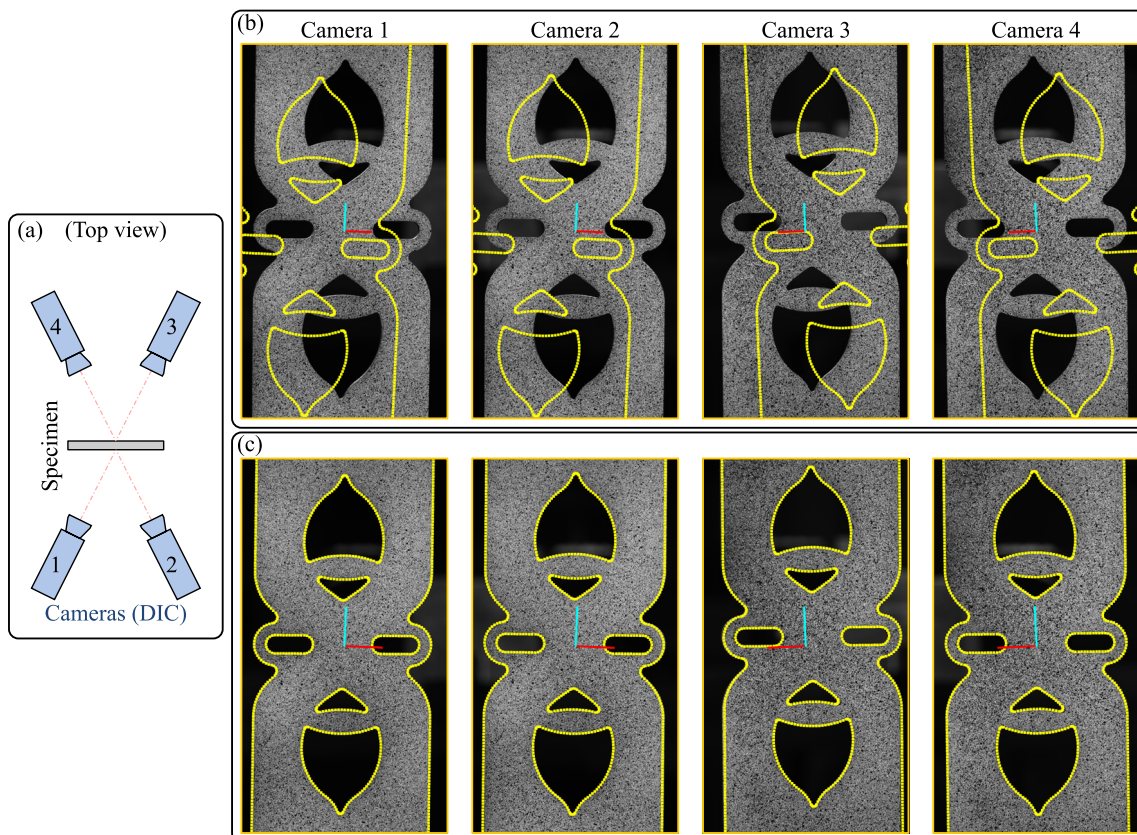


Fig. 12. Alignment of the specimen: a) camera arrangement, b) the initial misalignment and c) the optimal alignment

10^6 px^2 with the optimal values of the mapping parameters determined to be: $\hat{\alpha} = 2.108^\circ$, $\hat{\Delta x} = 4.907 \text{ mm}$, $\hat{\Delta y} = 3.091 \text{ mm}$.

The final result of alignment is shown graphically in Fig. 12. The corresponding Fig. 12a schematically presents the experimental set-up. The initial misalignment of the measured and modelling specimen shape is presented in Fig. 12b, shown in the measuring coord. system. The final alignment of specimens is presented in Fig. 12c. Although it is difficult to quantify the level of the alignment, practically no difference between the aligned shapes can be observed.

Handling of the artifacts. To test the ability of the method in handling geometrical mismatches (due to machining or manufacturing tolerances) we purposely misplaced the holes in the measured specimen in the first case, see the upper row in Fig. 13, Case A, where the artifacts are marked with red on the ideal shape shown in white. In the second case, Case B, the roundings on the outer contour were purposely modified to some extent on the measured specimen as if they were not properly machined. The initial position of the modelled specimen is shown with magenta dots. As can be seen in the lower row of the figure, the alignment was performed successfully in both cases.

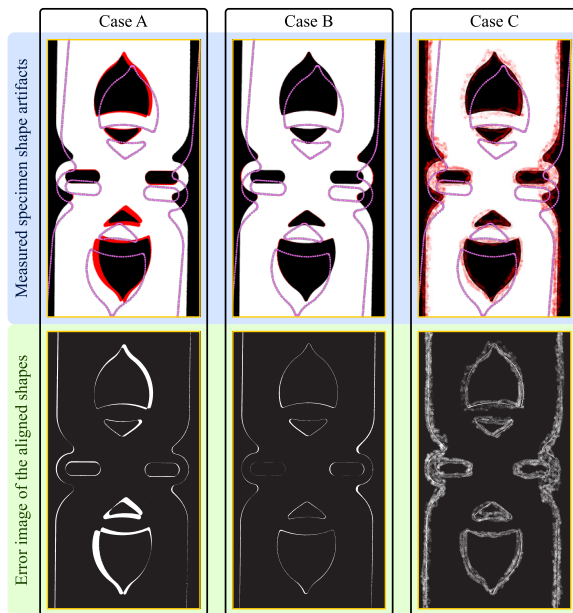


Fig. 13. Handling of the artifacts; upper row: the assumed artifacts, marked with red on the ideal specimen shape (white), initial modelled specimen shape position, marked with magenta, and lower row: the alignment results; Cases A and B analysed the mismatches in the measured geometry and Case C analysed the presence of noise (outliers)

The ability of the method to handle noise is analysed in Case C, where noise (outliers) are added along the entire contour of the measured specimen. As can be seen in the lower row of the figure, the method managed to successfully perform the alignment. We have also analysed the assumed cases with the ICP method. In Cases A and B, ICP performed the alignment as the proposed method whereas in Case C, the ICP method diverged.

3 DISCUSSION

The purpose of this study was to present a new methodology for aligning full-field measurements. More specifically, the method deals with the alignment of planar specimens, which is a field becoming increasingly popular due to its potential when combining full-field measurements with material characterization. As presented in [22], by using the full-field measurement techniques and monitoring the specimen loads, it is possible to characterize the anisotropic material behaviour from a single heterogeneous strain field specimen by employing inverse identification techniques (eq. finite element model updating, virtual fields method). However, as pointed out in the introduction, the outcome of the material characterization process crucially depends on the accuracy of the alignment between the measured and modelling data.

In the first example, the method was applied to a synthetic experiment. The shape of the specimen resembled a structure of a metamaterial. The example was chosen due to its periodic structure which can cause difficulties in the aligning procedure. We analyse the initial misalignment effect and the performance of the method compared with the ICP algorithm. The results demonstrated the robustness of the proposed method, which managed to successfully perform the alignment even at 90° of the initial rotation. This was not the case for ICP, which managed to perform the alignment up to 45° of the initial rotation only. We need to point out, however, that only the most basic version of the closed-form ICP was employed in this work. There are numerous modifications of the method [23] that could perform better. On the other hand, the performance of the proposed method could also be enhanced, such as by using pixels weights or by modifying the optimization algorithm. By employing such modifications, it is possible to successfully perform the alignment for the entire region of initial misalignments in Fig. 6 (data omitted). However, as is the case with the ICP, the convergence of the proposed

alignment algorithm cannot be guaranteed in a general case.

In the majority of cases on which we tested alignment methods, the performance of the ICP and the proposed method was comparable. In general, the advantage of the ICP is its computation efficiency. The method uses singular value decomposition (SVD) for the computation of alignment parameters whereas in the proposed approach an optimization approach is assumed. However, the benefit of the method is its robustness. As demonstrated with the first example, the initial mismatch did not considerably affect the number of iterations whereas they significantly increase in the case of the ICP. This property of the proposed approach comes from using the entire specimen region for the error estimation whereas in the ICP only the contour of a specimen is assumed.

The accuracy of the proposed algorithm on the one hand depends on the quality of the measuring image and on the other on the accuracy of the calibration. The mapping between the observed and modelled geometry is a composite of two mappings. First mapping c_1 of images, provided by the cameras, onto the unified plane takes place, subsequently followed by the mapping f of these points onto the space of the modelled specimen. It is important to note that the alignment algorithm addresses only the latter because the former is defined during a calibration procedure of cameras, needed for any full-field measurement system.

In the second example, the specimen recognition and the alignment process were both demonstrated. It can be seen from the acquired specimen's images (Fig. 11) that a simple threshold effect for the contour recognition could not be employed. Due to the speckle pattern, there are similar values of brightness in the background as well as on the specimen. For the presented approach of shape recognition, however, this was not an issue. The alignment of the specimen was in the example performed by using the proposed approach. However, ICP or any other method could be employed as well. From analysing the example (data omitted), similar performance was obtained for both the ICP and the proposed method, with ICP being computationally more efficient. Methods were also analysed for dealing with image artifacts, such as noise and geometrical mismatches due to machining or manufacturing tolerances. In the case of handling the noise, the proposed method turned out to be superior, otherwise, it is known that the ICP algorithm is susceptible to such artifacts [24].

In comparison to alignment procedures published in the field of material characterisation [17] and

[18], the benefit of the proposed approach is that it needs no user input for the shape recognition or for the alignment procedure and it is fairly easy to be implemented. Although we cannot claim that the presented approach for solving the shape recognition and the alignment problem is novel since in both areas there are numerous publications, we found no studies in the field of material characterisation that would address both problems and join them in a form of a methodology.

4 CONCLUSIONS

An integral part of advanced material characterisation by using full-field measurement techniques is the alignment between the FEA data and the experimental DIC data. Despite numerous publications in the field of treating planar specimens, studies that address the subject are scarce.

In the paper, a methodology is presented that enables the alignment of data from a single measuring system. In practice, the alignment approach needs to be addressed once the specimen is placed in the measuring system, more precisely, it needs to be addressed by the measuring system used for the DIC itself. However, because DIC does not recognize the pattern near an object's contour, the location of the contour is not exactly known. With the presented methodology we address both problems, specimen shape recognition, and the alignment procedure. The practical application of the method is presented on two examples, which demonstrate the robustness of the method, its comparison with the ICP algorithm, and its application on real DIC data.

Although the results show that the methodology manages to successfully perform the alignment, it is difficult to actually quantify its accuracy (from both the shape recognition and the alignment process). Such an analysis can be performed by means of computing full-field error maps [10]. For the present methodology, this remains to be performed.

5 ACKNOWLEDGEMENTS

The authors acknowledge the financial support from the Slovenian Research Agency (research core funding No. P2-0263).

6 REFERENCES

- [1] Moayyedean, F., Kadkhodayan, M. (2015). Combination of modified Yld2000-2d and Yld2000-2d in anisotropic pressure dependent sheet metals. *Latin American Journal of Solids*

- and Structures, vol. 12, no. 1, p. 92-114, DOI:10.1590/1679-78251372.
- [2] Starman, B., Vrh, M., Halilović, M., Štok, B. (2014). Advanced modelling of sheet metal forming considering anisotropy and young's modulus evolution. *Strojniški Vestnik - Journal of Mechanical Engineering*, vol. 60, no. 2, p. 84-92, DOI:10.5545/sv-jme.2013.1349.
- [3] Grédiac, M., Hild, F., Pineau, A. (eds.) (2013). *Full-Field Measurements and Identification in Solid Mechanics*, John Wiley & Sons, Inc, Hoboken, DOI:10.1002/9781118578469.
- [4] Ruybalid, A.P., Hoefnagels, J.P.M., van der Sluis, O., Geers, M.G.D. (2016). Comparison of the identification performance of conventional FEM updating and integrated DIC. *International Journal for Numerical Methods in Engineering*, vol. 106, no. 4, p. 298-320, DOI:10.1002/nme.5127.
- [5] Kavanagh, K.T., Clough, R.W. (1971). Finite element applications in the characterization of elastic solids. *International Journal of Solids and Structures*, vol. 7, no. 1, p. 11-23, DOI:10.1016/0020-7683(71)90015-1.
- [6] Wang, D., Mottershead, J.E. (2016). Measurement precision and spatial resolution with Kriging digital image correlation. *Strojniški vestnik - Journal of Mechanical Engineering*, vol. 62, no. 7-8, p. 419-429, DOI:10.5545/sv-jme.2016.3736.
- [7] Thengade, A., Dondal, R. (2012). Genetic Algorithm - Survey Paper. IJCA Proceedings on National Conference on Recent Trends in Computing, p. 6.
- [8] Henderson, D., Jacobson, S.H., Johnson, A.W. (2003). The theory and practice of simulated annealing, Glover, F., Kochenberger, G.A. (eds.). *Handbook of Metaheuristics* (vol. 57), Kluwer Academic Publishers, Boston, p. 287-319, DOI:10.1007/0-306-48056-5_10.
- [9] Fehervary, H., Vastmans, J., Vander Sloten, J., Famaey, N. (2018). How important is sample alignment in planar biaxial testing of anisotropic soft biological tissues? A finite element study. *Journal of the Mechanical Behavior of Biomedical Materials*, vol. 88, p. 201-216, DOI:10.1016/j.jmbbm.2018.06.024.
- [10] Lava, P., Jones, E.M.C., Wittevrongel, L., Pierron, F. (2020). Validation of finite element models using full field experimental data: Levelling finite element analysis data through a digital image correlation engine. *Strain*, vol. 56, no. 4, art. ID 12350, DOI:10.1111/str.12350.
- [11] Polyga (2019). 3D Scanning flat objects, from <https://www.polyga.com/blog/3d-scanning-flat-objects/>, accessed on 2021-01-25.
- [12] Besl, P.J., McKay, D.N. (1992). A method for registration of 3-D shapes. *IEEE Transactions on Pattern Analysis and Machine Intelligence*, vol. 14, no. 2, p. 239-256, DOI:10.1109/34.121791.
- [13] Schutz, C., Jost, T., Hugli, H. (1998). Multi-feature matching algorithm for free-form 3D surface registration. *Proceedings. Fourteenth International Conference on Pattern Recognition* (Cat. No.98EX170), Vol. 2. p. 982-984, DOI:10.1109/ICPR.1998.711852.
- [14] Rusinkiewicz, S., Levoy, M. (2001). Efficient variants of the ICP algorithm. *Proceedings Third International Conference on 3-D Digital Imaging and Modeling*, p. 145-152, DOI:10.1109/IM.2001.924423.
- [15] Bing, J., Vemuri, B. C. (2011). Robust point set registration using gaussian mixture models. *IEEE Transactions on Pattern Analysis and Machine Intelligence*, vol. 33, no. 8, p. 1633-1645, DOI:10.1109/TPAMI.2010.223.
- [16] Eggert, D.W., Lorusso, A., Fisher, R.B. (1997). Estimating 3-D rigid body transformations: a comparison of four major algorithms. *Machine Vision and Applications*, vol. 9, no. 5-6, p. 272-290, DOI:10.1007/s001380050048.
- [17] Bruno, L., Furguele, F.M., Pagnotta, L., Poggialini, A. (2002). A full-field approach for the elastic characterization of anisotropic materials. *Optics and Lasers in Engineering*, vol. 37, no. 4, p. 417-431, DOI:10.1016/S0143-8166(01)00120-8.
- [18] Silva, G.H.C. (2009). *Identification of Material Properties Using Finite Elements and Full-Field Measurements with Focus on the Characterization of Deterministic Experimental Errors*. Ecole des Mines de Saint Etienne, Saint Etienne.
- [19] Souto, N., Andrade-Campos, A., Thuillier, S. (2016). A numerical methodology to design heterogeneous mechanical tests. *International Journal of Mechanical Sciences*, vol. 107, p. 13, DOI:10.1016/j.ijmecsci.2016.01.021.
- [20] Yoneyama, S., Kikuta, H., Kitagawa, A., Kitamura, K. (2006). Lens distortion correction for digital image correlation by measuring rigid body displacement. *Optical Engineering*, vol. 45, no. 2, p. 9, DOI:10.1117/1.2168411.
- [21] Mirzaali, M.J., Janbez, S., Strano, M., Zadpoor, A.A. (2018). Shape-matching soft mechanical metamaterials. *Scientific Reports*, vol. 8, art. ID 965, DOI:10.1038/s41598-018-19381-3.
- [22] Maček, A., Starman, B., Mole, N., Halilović, M. (2020). Calibration of Advanced yield criteria using uniaxial and heterogeneous tensile test data. *Metals*, vol. 10, no. 4, art. ID 542, DOI:10.3390/met10040542.
- [23] Liu, Y. (2004). Improving ICP with easy implementation for free-form surface matching. *Pattern Recognition*, vol. 37, no. 2, p. 211-226, DOI:10.1016/S0031-3203(03)00239-5.
- [24] Gao, W., Tedrake, R. (2019). FilterReg: Robust and Efficient Probabilistic Point-Set Registration using Gaussian Filter and Twist Parameterization. *2019 IEEE/CVF Conference on Computer Vision and Pattern Recognition (CVPR)*, p. 11087-11096, DOI:10.1109/CVPR.2019.01135.